J Mater Sci (2008) 43:3253–3258
DOI 10.1007/s10853-008-2540-2

The liquid metastable miscibility gap in the Cu–Co–Fe system

Stefano Curiotto · Livio Battezzati · Erik Johnson · Mauro Palumbo · Nini Pryds

Received: 11 June 2007 / Accepted: 7 February 2008 / Published online: 11 March 2008

Abstract Cu–Co–Fe alloys undercooled below a certain temperature display demixing of the liquid, followed by coagulation before dendritic solidification. In this article high temperature phase equilibria in Cu–Co–Fe samples have been precisely determined by DSC. Special attention has been paid to the liquid–liquid phase separation and on its effect on the formation of microstructures. The measured transformation temperatures have also been used to update the description of the ternary phase diagram.

Introduction

Cu-based alloys such as Cu–Fe and Cu–Co display a liquid separation in the undercooled melt and their phase diagram is characterized by a liquid metastable miscibility gap. A considerable amount of work has been published on these two alloy systems in order to study the liquid phase separation and to assess the position of the miscibility gap [1–5]. Also, the ternary Cu–Co–Fe displays metastable liquid demixing, but less information is available in the literature on this system. Early investigations on the Cu–Co–Fe stable equilibria were performed by Jellingahus [6] and Maddocks and Clausen [7]. They drew vertical sections of the phase diagram using experimental data obtained by thermal analysis and metallography. Kim and Abbaschian [8] measured liquidus and demixing temperatures of several Cu–Co–Fe alloys by means of a pyrometer. They also showed the microstructures of samples which displayed a separation in the liquid state. Bamberger et al. [9] processed Cu–Co–Fe alloys with different compositions by Electromagnetic Levitation and measured the related melting temperatures. Their data differ from those of other authors by more than 100 K, probably because of the low sensitivity of the experimental technique used. Precise measurements of liquidus and demixing temperatures were carried out by means of differential thermal analysis (DTA) by Cao et al. [10]. They experimentally determined boundaries of the ternary liquid miscibility gap showing quasi-binary sections of the phase diagram. All the experimental data available in the literature were recently collected by Palumbo et al. [11] who optimized the description of the Cu–Co–Fe phase diagram. They also presented a new assessment of the binary Cu–Co system. Using the CALPHAD (CALculation of PHAse Diagram) approach, a significant improvement in the description of the metastable miscibility gap with respect to previous thermodynamic calculations was achieved. However, the calculation of the phase diagram could be further improved, in particular as regards the description of the liquidus curve.

S. Curiotto · L. Battezzati · M. Palumbo
Dipartimento di Chimica IFM, Centro di Eccellenza NIS, Università di Torino, Via Giuria 9, 10125 Torino, Italy

Present Address:
S. Curiotto (✉)
CINaM-CNRS, Campus de Luminy, Case 913, 13288 Marseille, France
e-mail: stefano.curiotto@unito.it

E. Johnson
Niels Bohr Institute, Nanoscience Centre, University of Copenhagen, Copenhagen, Denmark

E. Johnson
Materials Research Department, Risoe National Laboratory, Frederiksborgvej 399, DK-4000 Roskilde, Denmark

N. Pryds
Fuel Cell and Solid State Chemistry Department, Risoe National Laboratory, Frederiksborgvej 399, DK-4000 Roskilde, Denmark

In the present work the transformation temperatures of several selected Cu–Co–Fe alloys with different compositions have been measured by differential scanning calorimetry (DSC). After DSC processing, the calorimetric signals have been related to the microstructures of the alloys studied by scanning electron microscopy (SEM) and the mechanism of coagulation during liquid demixing has been disclosed. The experimental transition temperatures obtained by DSC have been used to re-optimize the liquid phase of the Cu–Co–Fe system in order to improve the description of liquidus and demixing curves.

Experimental and modelling details

High purity copper (99.999%), cobalt (99.9%) and iron (99.98%) have been pre-alloyed in the desired proportion to attain different compositions in an arc-melting furnace (see Table 1). The weight of the pure elements was checked with a precision of 0.1 mg. Before melting the chamber has been evacuated and purged several times with high purity Ar and using lumps of Zr as getter. Each sample had a weight between 150 and 250 mg. In order to check for any loss of the elements (e.g. by evaporation) and consequent deviation from the chosen composition, after melting the alloys have been weighed. The loss of mass has always been less than 0.3 mg, i.e. well below 1%. The content of carbon and sulphur in selected alloys were measured by means of a LECO analyzer, as they can affect the liquid miscibility gap. They resulted to be as low as 0.0033 and 0.0025 wt%, respectively.

In order to avoid oxidation, each specimen has been inserted in an alumina crucible with about 50 mg of crushed Duran glass which is used as fluxing agent. The DSC experiments have been carried out in two different instruments, a Netzsch DSC 404 C and a Setaram HTDSC, calibrated with the melting temperatures of pure In, Zn, Ag, Au and Ni. For the Netzsch instrument, instead of the melting point of pure Ni, the fcc to bcc transition of pure Fe has been used, because of oxidation of Ni. For each composition, one to four samples have been processed several times, with heating and cooling rates ranging between 2 and 40 K/min. In order to allow better homogenization of the alloy in the liquid state, an isothermal step of 5–10 min has been held at the end of each heating run above the liquidus temperature; this temperature depends on the composition of the specimen. After the DSC processing, the solidified samples have been mounted in resin, cross-sectioned and polished (without etching) to be observed by SEM in backscattering mode. The microscope used is a Jeol 840 SEM, equipped with an Energy Dispersive Spectroscopy (EDS) microprobe.

The transformation temperatures measured by DSC have been used to assess the ternary phase diagram by means of the CALPHAD approach. The calculations have been performed using the ThermoCalc software package [12]. The excess free energy of mixing for a certain phase φ has been expressed as follows:

$$
\begin{aligned}
{}^{ex}G^{\varphi} = {} & x_{Co}x_{Cu}L^{\varphi}_{Co,Cu} + x_{Co}x_{Fe}L^{\varphi}_{Co,Fe} + x_{Cu}x_{Fe}L^{\varphi}_{Cu,Fe} \\
& + x_{Co}x_{Cu}x_{Fe}\left(x_{Co}\cdot {}^{0}L^{\varphi}_{Co,Cu,Fe} + x_{Cu}\cdot {}^{1}L^{\varphi}_{Co,Cu,Fe}\right. \\
& \left. + x_{Fe}\cdot {}^{2}L^{\varphi}_{Co,Cu,Fe}\right)
\end{aligned}
$$

where the binary interaction parameters are:

$$
L^{\varphi}_{i,j} = \sum_{v=0}^{n} {}^{v}L^{\varphi}_{i,j}(x_i - x_j)^{v}
$$

The L parameters can be temperature dependent. Further details on the thermodynamic modelling are reported in our previous work [11].

Results and discussion

Differential scanning calorimetry

In Fig. 1 a DSC curve of a $Cu_{50}Co_{12.5}Fe_{37.5}$ is shown as an example of the full processing cycle. The transformations

Table 1 Temperatures in K of the transformations occurring during differential scanning calorimetry for each investigated alloy

Alloy	at.% Cu	at.% Co	at.% Fe	Eutectoid		Peritectic		Liquidus		Demixing	
				Measured	Calculated	Measured	Calculated	Measured	Calculated	Measured	Calculated
a	90	5	5	1,219 ± 4	1,196	1,368 ± 4	1,369	1,577 ± 25	1,583	1,456 ± 3	1,498
b	50	25	25	1,214 ± 1	1,193	1,370 ± 3	1,369	1,669 ± 13	1,682	1,618 ± 1	1,609
c	50	12.5	37.5	1,212 ± 6	1,191	1,366 ± 4	1,370	1,687 ± 5	1,689	1,637 ± 2	1,629
d	50	37.5	12.5	/	643	1,374 ± 7	1,372	1,670 ± 7	1,668	1,591 ± 3	1,577
e	25	30	45	1,219 ± 5	1,202	1,368 ± 3	1,369	1,693 ± 13	1,721	1,569 ± 1	1,581
f	25	65	10	/	919	1,377 ± 4	1,374	1,688 ± 16	1,705	1,514 ± 4	1,494
g	25	10	65	1,163 ± 12	1,165	1,366 ± 5	1,371	1,711 ± 9	1,723	1,601 ± 2	1,592
h	12	22	66	1,209 ± 2	1,190	1,367 ± 1	1,370	1,727 ± 1	1,748	1,444 ± 1	1,473
i	12	44	44	1,224 ± 3	1,192	1,364 ± 7	1,369	1,715 ± 1	1,742	–	1,450

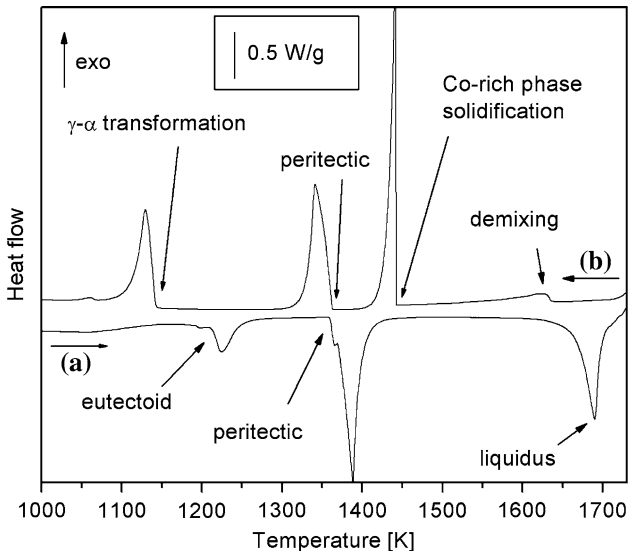

Fig. 1 DSC signals of a $Cu_{50}Co_{12.5}Fe_{37.5}$ alloy on heating and cooling (see arrows). Heating and cooling rate: 40 K/min

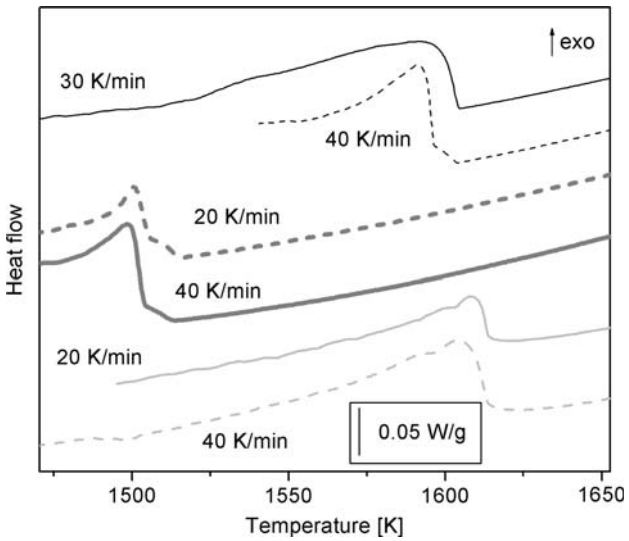

Fig. 2 Demixing signals in $Cu_{25}Co_{10}Fe_{65}$ (thin black line, 30 and 40 K/min), $Cu_{25}Co_{65}Fe_{10}$ (thick gray line, 20 and 40 K/min) and $Cu_{50}Co_{25}Fe_{25}$ (gray line, 20 and 40 K/min)

of the sample during heating and cooling can be followed along curves a and b, respectively. They have been understood comparing the DSC signals with those obtained in Cu–Co and Cu–Fe alloys and in relation with preliminary calculations of the ternary phase diagram. The measured transformation temperatures for each investigated alloy are reported in Table 1. The experimental data are an average of the temperatures found in several runs with the two DSC instruments used. The compositions $Cu_{50}Co_{12.5}Fe_{37.5}$ and $Cu_{50}Co_{37.5}Fe_{12.5}$ were studied also by Cao and Görler [10]; the differences between their transformation temperatures and those measured in this work are less than 5 K, indicating a good agreement between the two sets of measurements.

As can be seen in Fig. 2, in (Co,Fe)-rich alloys the liquid phase separation occurs often with two onsets, as found and explained in Co-rich Cu–Co samples [13]. The demixing of the Cu-rich liquid, which has lower interface energy with the glass than the Co-rich liquid, should start with heterogeneous nucleation at the interface between alloy and glass. Far from this surface, separation of the Cu-rich liquid occurs at a slightly lower temperature, in order to reach the equilibrium described by the binodal. However, at fixed composition, the first onset of demixing occurs always at the same temperature regardless of the cooling rate. Then the liquid phase separation takes place with no detectable undercooling below the miscibility gap (see Fig. 2) thus confirming the result obtained in Cu–Co [4, 14] and opposite to that reported in [5] for Cu–Fe. In samples processed without fluxing the liquid–liquid separation was observed only rarely because solidification occurred in advance.

For the composition $Co_{10}Cu_{25}Fe_{65}$, a small exothermic peak ending at 1,480 ± 9 K has been found during heating (see Fig. 3) after the peritectic reaction. A similar peak has been observed in $Cu_{17}Co_{83}$ [14]. It was therefore suggested that the offset of the signal indicates the end of the solidification of the alloy during heating because of the retrograde solubility in the Co-rich phase of the Cu–Co system. Also, in the Cu–Co–Fe the solubility of the (Co,Fe)-rich phase is retrograde, therefore, the DSC peak observed during heating between peritectic and melting in the present work can be related to the completion of the solidification of the sample.

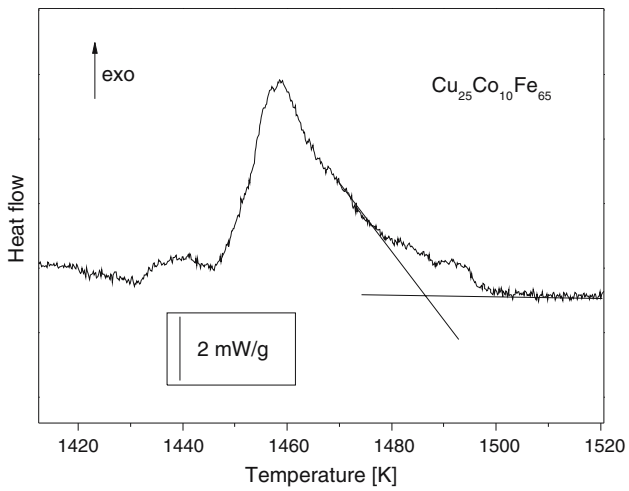

Fig. 3 Exothermic peak due to solidification of the sample after the peritectic reaction during heating of $Co_{10}Cu_{25}Fe_{65}$

Microstructures

In Fig. 4, a section of a $Cu_{50}Co_{12.5}Fe_{37.5}$ sample after DSC processing is shown as an example of the solidification microstructure after liquid separation. The image has been taken by SEM in backscattering mode, so the dark regions are (Co,Fe)-rich, the bright ones are Cu-rich. A large (Co,Fe)-rich sphere is surrounded by a Cu-rich matrix which contains several (Co,Fe)-rich dendrites. In all the demixed alloys the microstructure is found to be similar but the relative volume fractions between the two phases is different. During the demixing, droplets of the minority phase nucleate, grow and coagulate to reduce the interface energy with the other liquid phase [15]. The final microstructure is then a sphere of one phase embedded in the other one. The Cu-rich phase always constitutes the external layer because of the low interface energy between it and the molten glass used to avoid oxidation [4]. Similar microstructures have been observed in binary Cu–Co and Cu–Fe alloys processed by DSC [4, 5, 16].

In some samples the sphere of Co-rich phase appears to be composed of several small droplets separated one from the other by a thin Cu-rich layer, it is the case of $Cu_{50}Co_{37.5}Fe_{12.5}$ whose microstructure is shown in Fig. 5. In fact, the droplets form because of demixing and move towards the centre of the sample, which is warmer, because of Marangoni motion; meanwhile the temperature drops. In the upper part of the miscibility gap, a small change of temperature causes a large change in the compositions of the two liquid phases. Therefore, the droplets, in order to follow the equilibrium defined by the binodal, expel excess Cu towards the interface, delaying coagulation. The solidification, occurring 78 K below the demixing, freezes the microstructure.

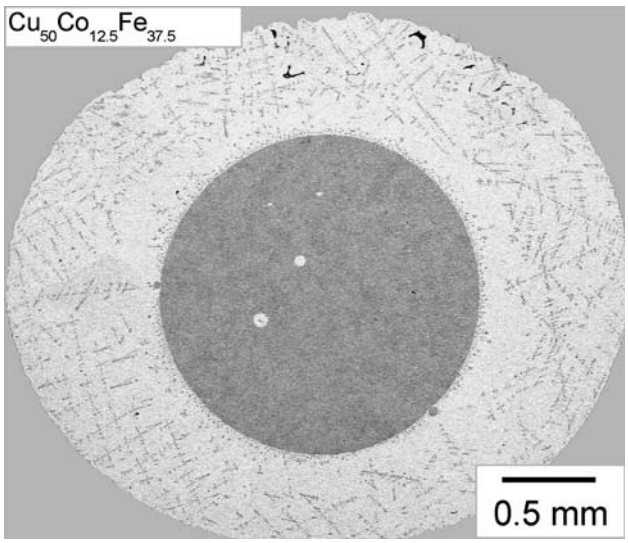

Fig. 4 SEM image obtained by backscattered electrons of a $Cu_{50}Co_{12.5}Fe_{37.5}$ processed by DSC. Dark regions are (Co,Fe)-rich; bright regions are Cu-rich. The sample experienced liquid phase separation: a large (Co,Fe)-rich sphere is inside a Cu-rich phase. Solidification occurred 194 K below the demixing temperature

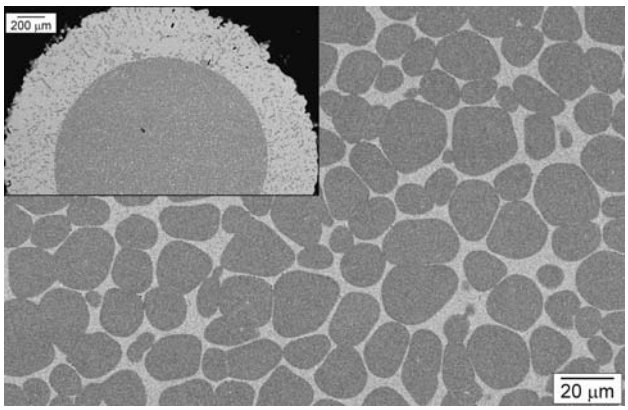

Fig. 5 SEM image obtained by backscattered electrons of a $Cu_{50}Co_{37.5}Fe_{12.5}$ processed by DSC, solidified 78 K below the demixing temperature. Dark regions are (Co,Fe)-rich; bright regions are Cu-rich. An overview of the whole sample is shown in the insert, while the main image shows a magnification of the central (Co-Fe)-rich phase

In samples where solidification occurs after undercooling of more than 100 K below the binodal, like in $Cu_{50}Co_{12.5}Fe_{37.5}$ shown in Fig. 4, the droplets result less separated. In fact their coagulation goes on also at low temperatures where the binodal is steep and their composition does not change much. So, the gradient in Cu concentration is flattened with elapsing time and does not restrain to coagulation anymore.

In a $Cu_{50}Co_{25}Fe_{25}$ alloy, solidification of the (Co,Fe)-rich phase took place only 9 K below the demixing temperature, the microstructure is shown in Fig. 6. After

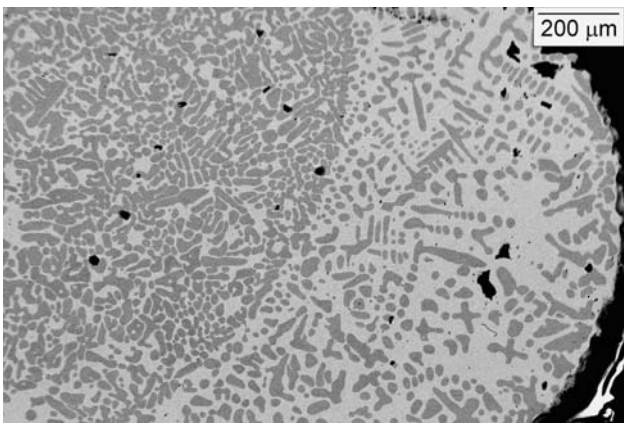

Fig. 6 SEM image obtained by backscattered electrons of a $Cu_{50}Co_{25}Fe_{25}$ processed by DSC, solidified 9 K below the demixing temperature. Dark regions are (Co,Fe)-rich; bright regions are Cu-rich. The sample experienced liquid phase separation: a (Co,Fe)-rich region on the left is separated by a curved interface from a phase richer in Cu on the right. The black spots are holes due to shrinkage

beginning of demixing and coagulation in the core of the sample, the two liquid phases are still rather concentrated in the respective solutes. Then the undercooled (Co,Fe)-rich fcc phase, which is prone to dendritic solidification, solidifies expelling the excess liquid Cu. The composition of the Cu-rich liquid must be that defined by the liquidus curve, thus the excess Co and Fe solidify. Therefore, dendrites are present in large amount in the external part of the sample and are also found in its core where otherwise, at higher undercooling, droplets solidify retaining their shape (Fig. 5).

Comparison of Figs. 4 to 6 clearly shows the effect of undercooling on the demixing and coagulation processes. At low undercooling (Fig. 6) Co droplet movement towards the centre of the sample has started but there are still large Cu zone in the same area allowing for dendritic solidification. At intermediate undercooling (Fig. 5) the Co-rich droplets have approached each other and must have reached a metastable mechanical equilibrium. The equilibrium is metastable because of the excess amount of surfaces in the sample, but stable enough in time since various interfaces appear flat, as if the droplets were pushed close together. From this it is deduced that these liquids are rather quiescent and there is little movement in the sample which could promote the breaking of interfaces and further coagulation. It must be noted that the interfacial zones seen in the figures, must have been thinner at high temperature because they must have grown in thickness during the peritectic reaction. It is only at the highest undercooling (Fig. 4) that coagulation has proceeded to a large extent.

Energy dispersive spectroscopy

EDS measurements have been performed on the samples processed by DSC. In Table 2 the compositions of the (Co,Fe)-rich and of the Cu-rich phase are shown for each alloy. The reported values are an average of 10 spot measurements in different points of the same phase. The composition of the dendrites, within the experimental error, is always equal to that of the (Co,Fe)-rich spheres. The Cu-rich phase is constituted of almost pure Cu, while in the (Co,Fe)-rich phase there is still much Cu because, after the solidification, the system does not follow the equilibrium. As explained in [18], the diffusion in the solid phase is slow, therefore, the composition of the (Co,Fe)-rich phase does not change much from the solidification temperature to room temperature. The penetration of the electron probe used for EDS analysis is high with respect to the small Cu-rich droplets of alloy *h*, therefore its composition values should be considered with caution.

Table 2 Compositions, measured by EDS, of the Cu-rich and (Co,Fe)-rich phases after DSC processing. The error on the measurement is 1.0%

Alloy	Cu-rich phase			Co-rich phase		
	at.% Cu	at.% Co	at.% Fe	at.% Cu	at.% Co	at.% Fe
a	96.0	2.0	2.0	11.0	45.0	44.0
b	95.7	1.9	2.4	16.0	42.0	42.0
c	97.9	0.6	1.5	7.7	24.2	68.1
d	94.9	4.0	1.1	11.4	64.8	23.8
e	96.7	1.5	1.8	11.0	34.6	54.4
f	97.0	2.7	0.3	11.0	77.0	12.0
g	96.9	1.1	2.0	12.6	12.6	74.8
h	85.0	5.0	10.0	13.0	22.4	64.6
i	Not demixed					

Optimization of the Cu–Co–Fe liquid phase

As new experimental data have been made available in this work, the ternary phase diagram we recently assessed [11] has been updated by revising the thermodynamic description of the Cu–Co–Fe liquid phase. With this it was hoped to resolve some discrepancies between experimental data and the previous assessment. For instance, $Cu_{12}Co_{22}Fe_{66}$ shows liquid demixing at 1,444 K, temperature much lower than that predicted by the previously calculated phase diagram (1,500 K). This indicates that the description of the liquid miscibility gap in the phase diagram can be improved. The solid phases have not been optimized because the solid equilibria were already well described by a wealth of data. Lattice stabilities and magnetic properties of pure elements are taken from [17]. Binary interaction parameters are taken from [11], [18] and [19] for Cu–Co, Cu–Fe and Co–Fe, respectively.

Final values of the assessed ternary parameters of the liquid are reported in Table 3. These substitute for those given in [11], whereas the other parameters remain unchanged. The calculated transformation temperatures are compared with the measured values in Table 1. The calculated eutectoid temperatures are slightly lower than the measured ones; this comes from the slight underestimation of the eutectoid temperature in [18]. The peritectic equilibria are very well approximated. Figure 7 shows a vertical section of the calculated ternary phase diagram together with the experimental data measured in the present work and in [10]. With the present description of the liquid phase, the liquidus curve is closer to the experimental data

Table 3 Thermodynamic ternary interaction parameters for the Cu–Co–Fe liquid phase evaluated in this study

${}^{0}L^{\text{liquid}}_{\text{CO,Cu,Fe}}$	4,930
${}^{1}L^{\text{liquid}}_{\text{CO,Cu,Fe}}$	−42,450
${}^{2}L^{\text{liquid}}_{\text{CO,Cu,Fe}}$	6,400

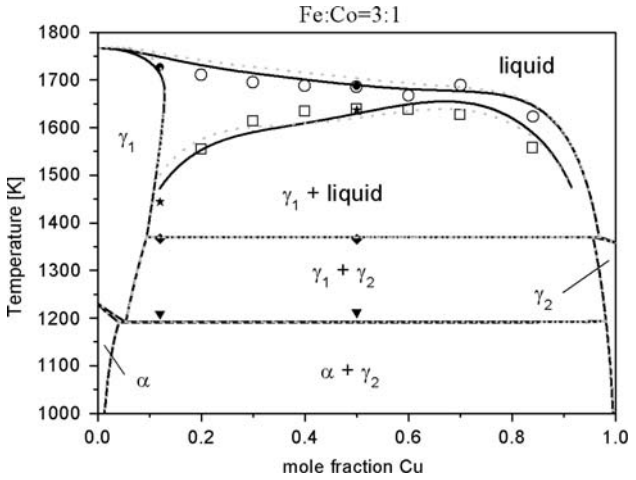

Fig. 7 Vertical section of the Cu–Co–Fe phase diagram (continuous line) calculated with constant ratio Fe:Co = 3:1. The previous calculation [11] is shown as dotted line. Experimental points are also reported for comparison. ◯, liquidus, Cao et al. [10]; ●, liquidus, this work; □, miscibility gap Cao et al. [10]; ★ miscibility gap, this work; ▼, eutectoid, this work; ◆, peritectic, this work; - - - - -, previous assessment [11]; ——, current assessment

and is therefore better assessed than in [11]. The metastable miscibility gap fits well the data points at the edges and is slightly high at compositions between 60 and 80 at.%Cu, contrary to the previous assessment. It predicts a maximum of the miscibility gap around 70 at.%Cu (Fig. 7) while it should occur at lower Cu content to approximate better the data. This is, however, believed to be the best possible description of the liquid phase to date. In fact, we tried to further correct the calculated binodal by changing manually the thermodynamic parameters of the liquid phase and forcing the gap to fit the measured points. Nevertheless, as a consequence of this, the liquidus curve moves to higher temperatures and is therefore not acceptable. It is believed that the problem might be due to the value of the binary interaction parameters of the Co–Fe system which appear to induce excessive lowering of the free energy of the liquid phase. Revising such binary diagram is outside the scope of this work.

Conclusions

Several Cu–Co–Fe alloys have been carefully investigated using different techniques. Their transformation temperatures have been precisely measured by DSC. By means of glass fluxing, high undercoolings of the melt have been obtained, allowing the study of the metastable liquid phase separation. With a thorough SEM and EDS analysis of the samples, the effect of demixing and solidification on the formation of the microstructures has been disclosed with clear emphasis on the role of undercooling. The description of the Cu–Co–Fe phase diagram has been updated using the new available experimental data, in order to enhance the description of the liquidus curve and of the liquid miscibility gap.

Acknowledgements The work has been supported by the European Space Agency within the project CoolCop (ESA-MAP AO 99–010). A. Ziggiotti (Centro Ricerche Fiat, Orbassano, TO, Italy) is gratefully acknowledged for the measurement of carbon and sulphur in the alloys.

References

1. Nakagawa Y (1958) Acta Metal 6:704
2. Battezzati L, Curiotto S, Pryds N, Johnson E (2006) Mater Sci Eng: A 449–451:7
3. Elder S, Munitz A, Abbaschian G (1989) Mater Sci Forum 50:137
4. Cao CD, Görler G, Herlach D, Wei B (2002) Mater Sci Eng: A 325:503
5. Wilde G, Willnecker R, Nandan Singh R, Sommer F (1997) Z Metallkd 88:804
6. Jellingahus W (1936) Archiv fur das Eisenhuttenwesen 10:115
7. Maddocks W, Clausen G (1936) Iron and steel institute, London, Special Report 14:116
8. Kim DI, Abbaschian R (2000) J Phase Equilib 21:25
9. Bamberger M, Munitz A, Kaufman L, Abbaschian R (2002) Calphad 26:375
10. Cao CD, Görler G (2005) Chin Phys Lett 22:482
11. Palumbo M, Curiotto S, Battezzati L (2006) Calphad 30:171
12. Jönsson B, Sundman B, Ågren J (1993) Thermochim Acta 214:93
13. Curiotto S, Pryds N, Johnson E, Battezzati L (2007) Fluid Phase Equilib 256:132
14. Curiotto S, Pryds N, Johnson E, Battezzati L (2006) Metall Mater Trans 37:2361
15. Ratke L, Diefenbach S (1995) Mater Sci Eng: R 15:263
16. Wang CP, Liu XJ, Ohnuma I, Kainuma R, Ishida K (2002) Science 297:990
17. SGTE Pure Elements database ver. 3.00, 1991 updated from: A.T. Dinsdale Calphad 5:(1981) 317
18. Jannson A (1986) Report d73. Technical report, KTH, University of Stockholm, Sweden
19. Ohnuma I, Enoki H, Ikeda O, Kainuma R, Ohtani H, Sundman B, Ishida K (2002) Acta Mater 50:379